Journal of Solid State Electrochemistry (2023) 27:1701–1715
https://doi.org/10.1007/s10008-023-05503-z

REVIEW PAPER

Photoelectrochemistry of two-dimensional and layered materials: a brief review

Péter S. Tóth[1] · Ba Qianqian[1] · Csaba Janáky[1]

Received: 4 February 2023 / Revised: 2 April 2023 / Accepted: 4 April 2023 / Published online: 24 April 2023

Abstract

Two-dimensional (2D) materials have unique band structure and show a great promise for optoelectronic and solar energy harvesting applications. Photoelectrochemical (PEC) processes are intensively studied employing these materials, due to their high specific surface area, and the possibility of surface modification by defect engineering/catalyst deposition. The PEC activity of different 2D and layered materials was scrutinized for water oxidation/reduction and for inorganic ion oxidation by a statistical analysis to reveal any specific trends. Furthermore, some frequently studied performance improvement strategies (i.e., heterojunctions, tunnelling, and co−catalysts) are also discussed. Overall, exploring novel materials of 2D family, and new directions are both needed to initiate further discussions and additional research activity, which might enable to harness the full potential of these exciting materials.

Keywords Chalcogenides · Light harvesting · Nanoflakes · Photoelectrocatalysis · Heterojunction

Introduction

Conversion of solar energy to valuable chemicals or fuels is a promising approach to contribute solving the problems of global climate change and the depletion of fossil resources. Photoelectrochemical (PEC) methods are feasible for the conversion of basic chemical feedstocks (i.e., water, carbon dioxide, and nitrogen) to clean chemicals or alternative fuels such as, hydrogen, hydrocarbons, and ammonia, while harnessing solar energy [1–6]. The main element in this process is a semiconductor, which absorbs photons to generate charge carriers (electron−hole pairs), and thus requires to possess a high light absorption coefficient (10^4–10^5 cm^{-1}) over a broad wavelength range. Two-dimensional (2D) semiconductors have unique properties, such as high carrier mobility (10^2–10^5 cm^2 V^{-1} s^{-1}), tunable bandgap [7, 8], anisotropic carrier transport, and high specific surface area, making these materials attractive for PEC applications. From a practical perspective, 2D materials can be produced in a scalable manner at low cost [9–13], and they possess elemental abundance and remarkable stability against (photo) corrosion [14].

Research on transition metal dichalcogenide bulk single crystals dates back to the early 1980s, achieving high photocurrent density (in the range of 10 mA cm^{-2}) for the water splitting [15–19]. Since the discovery of graphene [20] more attention is dedicated to i) synthesis ('bottom−up') and preparation ('top−down') methods to obtain 2D materials, ii) seeking of novel 2D semiconductor materials, iii) novel PEC processes. Corresponding members of 2D materials family with PEC applications highlighted in Fig. 1.

In this review, we summarize the recent progress on the fundamental understanding and applications of 2D and layered semiconductors in PEC processes. Firstly, we investigate the 2D nature of such materials, and define some of their unique advantages, mostly in terms of the optoelectronic properties. Then, we discuss some preparation methods, and summarize their application in PEC processes. We cover both model reversible redox reactions and practically interesting processes, such as water splitting, CO_2, and N_2 reduction reactions. Finally, recently developed strategies for enhancing the performance of 2D semiconductors are presented: i) increase the number of active sites (alignment of

✉ Péter S. Tóth
toth.peter.sandor@chem.u-szeged.hu

✉ Csaba Janáky
janaky@chem.u-szeged.hu

[1] Department of Physical Chemistry and Materials Science, University of Szeged, Rerrich Sq. 1, Szeged H6720, Hungary

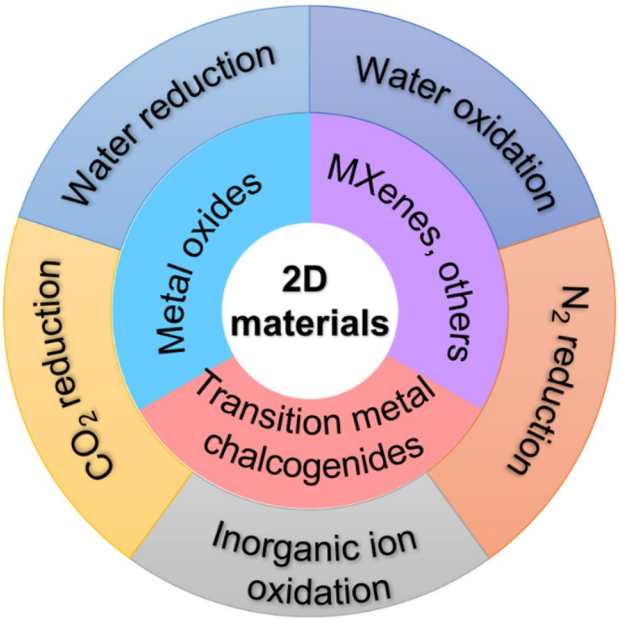

Fig. 1 Simplified overview of 2D materials and PEC applications covered by this review article

nanoflakes, defect passivation), ii) tuning the band structure (heterostructures, alloying, doping).

Definition of 2D materials

2D materials are atomically thin sheets with a high aspect ratio between their lateral size (µm-sized) and thickness (< 1 nm) [21]. In the corresponding bulk crystals with layered structure the neighboring layers are connected by van der Waals forces [22]. 2D materials include transition metal chalcogenides (TMCs), metal oxides, transition metal carbides, nitrides, carbonitrides (MXenes), and other materials. 2D TMCs with narrow bandgaps (1.09–1.89 eV) have suitable light absorption in the visible region and their bandgap can be tuned by changing the number of layers [23–25]. 2D TMCs with thin layers (few−to−monolayer) have a high specific surface area and a large portion of surface atoms, which could effectively reduce the distance of charge transport and accelerate PEC processes [26]. The monolayer nature can further assist the photogenerated carriers to reach the active sites and therefore reduce recombination. MXenes are a new type of 2D materials, composed of transition metal carbides and carbonitrides [27]. They have attracted notable attention and are widely studied in many fields, including catalysis, energy storage, and adsorption since their discovery in 2011 [28]. Figure 2A–F presents the morphology of nanoflakes, nanosheets and the film constructed from TMC sheets and metal oxides [29–32]. The optoelectronic properties (i.e., electronic band structure) of most 2D materials are thickness-dependent, because of the strong interlayer coupling and quantum confinement [33–37]. Figure 2G shows the bandgap change of SnSe as a function of the employed centrifugation speed during the synthesis [35], generally obtaining thinner flakes with higher centrifugation speed [38] (i.e., the bandgap is increasing with decrease of flake thickness). Additionally, Fig. 2H gives the same conclusion on the example of few-layer phosphorene with the number of layers (from 1 to 5L). In this case, the valence and conduction band edge positions are changing with the number of layers in the phosphorene few-layers [39].

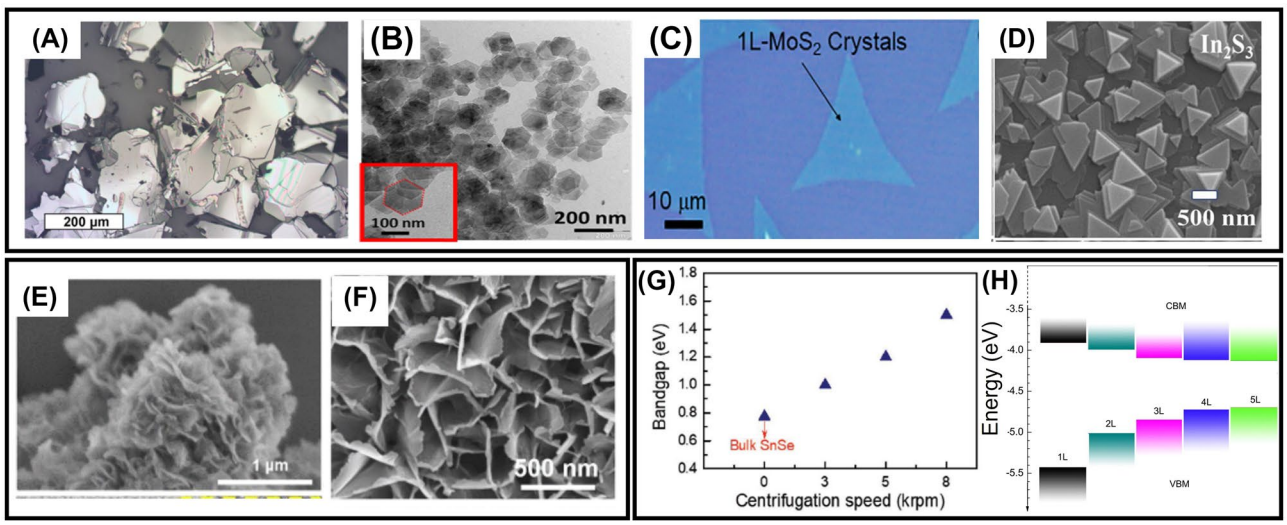

Fig. 2 Some examples of morphology of nanoflakes. **A** WSe_2, **B** SnS_2, **C** MoS_2, **D** In_2S_3, **E** CoV, **F** ZnO. **G** The change of SnSe bandgap as a function of the centrifugation speed. **H** Variation of valence band maximum (VBM) and conduction band minimum (CBM) positions of the 1L, 2L, 3L, 4L, and 5L of phosphorene determined from HSE06 calculation. Figures adapted with permission from: **A** [9] © 2017 American Chemical Society; **B** [29] © 2019 American Chemical Society; **C** [30] published by AIP Publishing under CC BY 4.0 license; **D** [31] © 2022 Elsevier; **E** [37] © 2022 John Wiley and Sons; **F** [32] © 2022 Elsevier; **G** [35] © 2019 John Wiley and Sons; **H** [39] published by Springer Nature under CC BY-NC-SA 4.0 license

Preparation methods for 2D nanoflakes and thin films

A variety of preparation methods have been developed towards the size and crystallinity control of 2D materials, and they can be categorized as bottom−up or top−down methods [40]. During the bottom−up approaches, the 2D materials are built up from either atoms or clusters to nanoscale structures [41]. For example, chemical vapor deposition, hydrothermal, and spray pyrolysis, can be used for producing 2D materials for commercial and research purposes, but at high cost, because of the required high temperature and vacuum [42–44]. In top−down methods, the 2D materials are obtained from their bulk counterparts, using mechanical, liquid-phase, or chemical exfoliation [41]. The materials yield and quality, however, highly depends on the exfoliation method. Mechanical exfoliation can produce high-quality nanosheets at low cost, but the yields are low, whereas liquid-phase exfoliation (LPE) gives a higher yield but at a higher cost [35, 40, 45].

In this review, we discuss 2D and layered semiconductors in two different configurations: i) nanoflakes prepared by any kind of exfoliation from the bulk counterpart, with lateral size of a few μm and the thickness in the range of several nm (e.g., mechanically exfoliated few-layer $MoSe_2$ flakes with ca. 11 nm thickness and hundred μm lateral size [46]), and ii) nanosheets or thin films, where the film is composed of the same material with large area (mm^2 or cm^2) and its thickness lies in the few−tens of nm range (e.g., 5 nm thick MoS_2 film deposited by thermolysis on p-Si wafer [47]). Table 1 summarizes the commonly used synthesis methods and the application of the as prepared 2D materials with some representative references [30, 48–50].

From a practical point of view, it is desirable to fabricate large−area and continuous thin films of 2D materials to further develop solar energy conversion devices. The Langmuir−Blodgett technique offers a versatile way to prepare layers/films in this regard. It consists of the transfer process of a water-insoluble material from the air−water interface onto a solid substrate, by dipping of the solid in the Langmuir monolayer [57]. Adding a stirring procedure during the film preparation [58], or depositing the film without Langmuir−Blodgett trough and film compression [59] can further extend the opportunities. Spin-coating is another conventional technique to fabricate thin layers of 2D materials [60]. As shown in Fig. 3A, first black phosphorus flakes were obtained by using electrochemically exfoliated bulk black phosphorus, and the flakes containing ink was spin-coated on indium tin oxide electrode [61]. A heating step was also introduced, which helps to remove solvent and eliminate the interlayer strain [45]. The film parameters, such as thickness and coverage, can be varied by the spin speed, spin-coating time, substrate size, and the amount of the ink [62].

Bottom−up methods can be employed to either directly grow film on substrate or to form the bulk material [42, 51, 54, 63]. For example, a $CuInS_2$ nanosheet was grown on a fluorine-doped tin oxide (FTO) coated glass, to form nanosheet films via the hydrothermal reaction, by putting clean FTO substrate into Teflon-lined stainless steel autoclave before starting the reaction [54].

Figure 3B shows that bulk $MoSe_2$ powder was obtained with direct vapor transport method, and subsequently was converted to multi−layer nanosheets by liquid-phase exfoliation, and then formed a $MoSe_2$ film on FTO by electrophoresis [12]. Chemical vapor deposition (CVD) is a commonly used approach to prepare 2D materials and films, because of the high-quality and yield of the forming products [31, 51, 52]. Another chemical vapor-phase approach is the atomic layer deposition (ALD), which can be employed to synthesize 2D materials using layer−by−layer growth with good thickness and uniformity control [55, 56, 64].

Table 1 The preparation methods of 2D materials

Strategy	Methods	Flakes Yield	Cost	Resulted Materials	Application	References
Top−down	Liquid-Phase Exfoliation	High	Moderate-high	TMCs/Oxides	Research/ commercial	[35, 45]
	Chemical Exfoliation	High	Moderate-high	Oxides/TMCs/MXenes	Research/ commercial	[41, 48]
	Mechanical Exfoliation	Low	Low	TMCs	Research	[26, 46]
Bottom−up	Chemical Vapor Deposition	High	High	TMCs/Oxides	Research/ commercial	[51, 52]
	Spray Pyrolysis	High	High	MXenes/Oxides	Research/ commercial	[50, 53]
	Hydrothermal Synthesis	High	Moderate-high	TMCs/Oxides	Research/ commercial	[3, 54]
	Atomic Layer Deposition	High	High	TMCs	Research/ commercial	[55, 56]

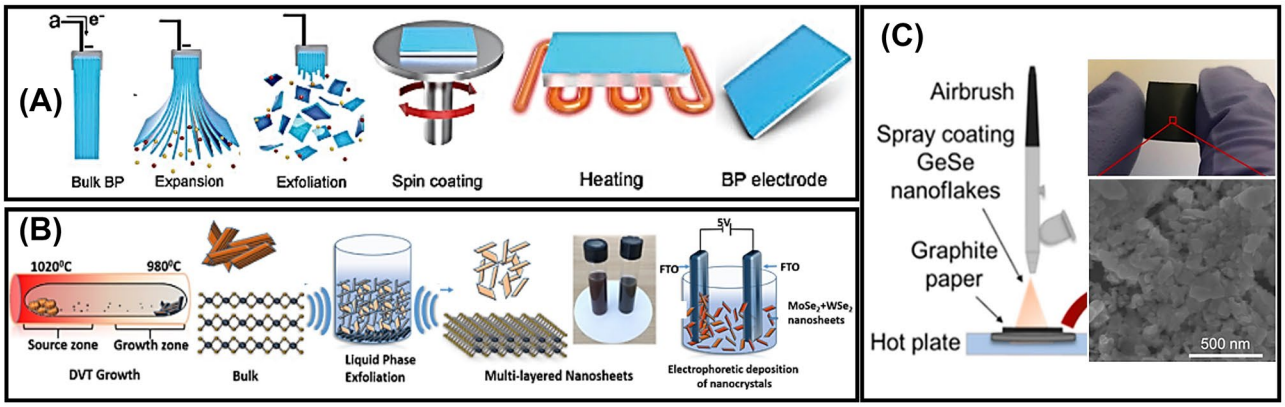

Fig. 3 **A** Illustration of the synthesis of black phosphorous nanosheets electrodes. **B** Schematic diagram of film formation on FTO prepared from bulk materials. **C** GeSe film produced by spray coating depositing the GeSe nanoflakes onto a graphite paper substrate, photograph of a GeSe photoelectrode, and its corresponding top−view SEM image. Figures adapted with permission from: **A** [61] © 2020, John Wiley and Sons; **B** [12] © 2019 American Chemical Society; **C** [65] published by American Chemical Society under CC BY 4.0 license

Spray coating is a widely employed technique to prepare films, allowing fast deposition of functional inks onto both rigid and flexible, large-area substrates [65–67]. Figure 3C shows the spray-coating of GeSe nanoflake suspension on a graphite paper [65] using an airbrush. A hotplate was employed to hold the substrate and evaporate the solvent, while also eliminating the interlayer strain during the spraying [45]. The material loading and the film thickness can be tuned by the number of spray coating cycles [68]. The right panels in Fig. 3C show the photograph of a GeSe photoelectrode and the morphology of GeSe film on graphite paper substrate. Notably, the parameters of the electrode preparation techniques determine the thickness, coverage, and orientation of nanoflakes in the film, also dictating their PEC activity.

To obtain 2D materials with specific properties, computational methods are frequently employed. For example, a series of 2D pentagonal transition metal dichalcogenides (2D sheets with pentagonal configuration), namely penta-MS_2 (M = Mn, Ni, Cu/Ag and Zn/Cd) monolayers were predicted using density functional theory [69]. Additionally, 2D structures were studied by theoretical calculations for CO_2 photoreduction [70]. In the case of stable monolayers, the proper bandgap, band edge positions, and surface reactivity have been predicted. Further theoretical work is needed to understand how defect engineering and surface treatments can be used to tune the PEC performance and enhance the reactivity.

Photoelectrochemical processes

The concept of PEC water splitting to produce hydrogen has been investigated for decades since the famous experiment of Fujishima and Honda in 1972 [71]. Semiconductors generate electron−hole pairs (charge carriers) when the illumination power is equal to or higher than their bandgap. In the case of photocathodes (p-type semiconductors), photoelectrons can transfer from the electrode surface driving the water reduction process (hydrogen evolution reaction—HER). The remaining holes go to the counterelectrode to perform the oxidation reaction. For n-type photoanodes, the charge carriers transfer occurs in the opposite direction, the holes can take part in the water oxidation reaction and electrons move to the counterelectrode to facilitate the reduction process [72, 73]. PEC CO_2 and N_2 reduction processes are similar to water reduction, but there are also considerable differences [2, 3, 74]. In CO_2 reduction, more products (CO, methane, ethylene, ethanol, etc.) are produced, and the product selectivity is mainly dependent on the selected catalysts and operating reduction potentials [75]. Additionally, inorganic ion oxidation, namely I^-, Br^-, S^{2-}, SO_3^{2-} oxidation reactions have lower standard redox potential than water oxidation [13, 44, 76, 77]. Figure 4 shows the histogram of the maximum photocurrent density values (recorded under 1 Sun irradiation) collected from the literature for H_2O reduction [51, 78–93], H_2O oxidation [31, 42, 86, 94–109], and inorganic ion oxidation reactions [13, 44, 63, 76, 77, 110, 111]. Only studies reporting photocurrent densities over 1 mA cm^{-2} were considered in our detailed analysis (see Fig. 4). As just a few reports were found on using 2D materials for PEC CO_2 and N_2 reduction [2–4, 37, 61, 74, 112–114], those are not analyzed here. Compared to the H_2O oxidation and inorganic ion oxidation reactions, the photocurrent densities recorded for the H_2O reduction reaction showed much broader distribution. The highest photocurrent value (i.e., 60 mA cm^{-2}) was obtained for MoS_2 in PEC water oxidation and reduction reactions under ca. 6 Sun illumination [115]. These results indicate that 2D materials can be applied for different PEC applications, both in oxidative and reduction reactions, and have ability to give higher performance in water reduction process than in the other ones.

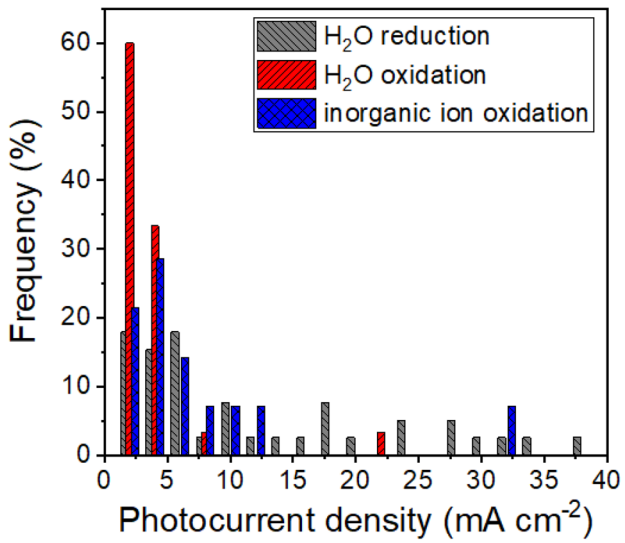

Fig. 4 Statistical analysis of maximum photocurrent density distribution (under 1 Sun)

Microelectrodes-based PEC studies

When applying 2D semiconductors in a photoelectrocatalysis, we have to consider the role of defects: steps, edges, cracks, atomic vacancies, anything, where the uniform crystal structure is missing or is modified. The importance of such defects has long been recognized in dictating the electrochemical (EC) behavior of layered materials. The general consensus assumes an increased EC activity of the edge (side or defected part of the 2D sheet) in comparison to the basal plane (smooth, uniform, defect-free part of the 2D sheet), although the exact reason of these differences is still being challenged [25, 46, 116–118]. In the case of bulk transition metal dichalcogenides, the basal plane and edge activity was studied extensively in the 1980s and 1990s [15, 16, 18, 19, 119]. Higher edge plane EC activity and lower PEC activity was found, compared to the basal plane of molybdenum and tungsten disulfides/diselenides. This trend was explained as defects, edges, which create surface states in the bandgap, act as recombination centers for the photogenerated charge carriers.

The revolution of 2D materials began in 2004 opened new avenues to understand the effect of structural domains for PEC activity, and to enhance the performance of these 2D semiconductors in photocatalytic processes. The heterogeneous electron transfer rate, the interfacial capacitance, and external quantum efficiency (EQE) have been studied using microscale EC/PEC approaches, including the scanning electrochemical microscopy, scanning electrochemical cell microscopy or microdroplet-based methods demonstrated the role of layer thickness, and structural domains (defects, terraces, edges) on their EC and PEC properties [26, 118, 120–128]. WSe_2 nanoflakes for example, have been investigated by scanning photocurrent microscopy in an electrochemical flow cell, and the photoconversion efficiency decreased on the edge sites because of the increased recombination of photogenerated charge carriers (Fig. 5A–D). LPE increases the defect density, and mostly, these defects refer to the increasing edge density. This trend can be explained by the increasing number of flakes and their decreasing lateral size as a result of the LPE process [118]. The spatial variation of the PEC performance of bare and Pt-decorated p-type WSe_2 photocathodes has also been studied, using in situ scanning photocurrent microscopy. This variation was attributed to a non-uniform distribution of surface and bulk defect states among terraces, particularly chalcogenide vacancies (Fig. 5E–H).

Notably, 2D materials produced by mechanical exfoliation have a large flake size with high purity, while the reproducibility is poor. Both flake and structural features – e.g., defect density – formation occur randomly, therefore a more precise synthesis method is needed. The effect of growth conditions during a chemical vapor-phase deposition of MoS_2 monolayers was studied, focusing on the defect formation. It was also scrutinized how these structural defects – point defects, dislocations, grain boundaries, and edges – could influence the electronic properties of the material [129]. These studies highlight the role of defects, and the use of activating agents (i.e., co-catalysts) to enhance the photocurrent density and incident photon−to−current efficiency (IPCE) values. They also help to uncover the mechanisms of charge carrier transfer and recombination in 2D semiconductors in a micrometer-scale.

Another body of knowledge accumulated on the effect of edges of MoS_2 monolayer on their EC HER properties [121, 130]. Significantly less attention has been dedicated to the PEC performance of 2D materials as a function of their structural features (Fig. 6A, B). The electron transfer kinetics on MoS_2 basal planes was accelerated with the growing number of layers, which was explained by the band structure-dependent photogeneration of charge carriers (Fig. 6C) [26].

We have recently observed the spatial variation of the PEC performance of $MoSe_2$ and WSe_2 photoanodes in the oxidation of a model redox couple (Fig. 6D–F) [46]. We have also shown that Pt nanoparticles obtained on p-WSe_2 nanoflakes by ALD result in a very high PEC activity in HER. Bulk defects and their migration to the surface were found to play an important role in the PEC activity enhancement. The W(VI) defects generated by heat treatment during the ALD process cause a decrease in the density of states near the valence band of WSe_2. The ALD deposited Pt nanoparticles i) nucleated primary on the W(VI) defects migrated to the surface, ii) their electron density compensates the decrease in the DOS of WSe_2 (Fig. 6A, B) [131].

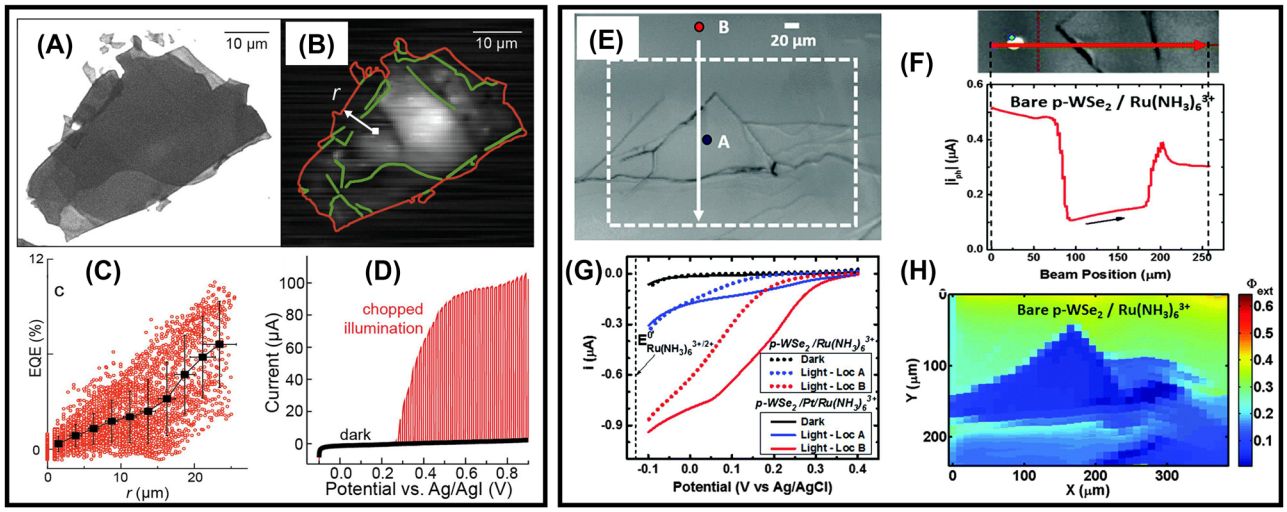

Fig. 5 **A** Bright−field transmission image of a single $MoSe_2$ nanoflake; **B**) EQE map for the nanoflake in (**A**), the red and green pixels represent perimeter edges and interior steps, respectively. The vector r represents the distance from a pixel in the EQE map to the nearest perimeter edge; **C** Plot of EQE vs. r for the nanoflake in (**A**). **D** Current−potential curves of a 1.3 mm^2 sized $MoSe_2$ single crystal in 1.0 M NaI, 1 mM I_2 electrolyte under dark (black line) and chopped 20 mW cm^{-2} 532 nm laser illumination (red line). **E** Optical image of a p-WSe_2 electrode; **F** Photocurrent measured as a function of beam position during a line scan as indicated by the white arrow in (**E**); **G** Linear sweep voltammograms obtained at locations **A** and **B** spots as indicated in (**E**) before and after platinization; **H** Two-dimensional map of EQE for area marked by the dotted rectangle in (**E**) [120]. Figures adapted with permission from: **A**–**D** [118] © 2018 American Chemical Society; **E**–**H** [120] published by Royal Society of Chemistry under CC BY-NC 3.0 license

Macroelectrode-based photoelectrochemical studies

In general, the increase of the photoelectrode area from micrometer-scale to mm^2 or cm^2 size causes a dramatic decrease in the photocurrent (to the μA cm^{-2} range) because of the abundant defects [24, 90, 132]. At the same time, regarding to the eventual development of solar energy conversion devices based on 2D materials, it is needed to prepare macroelectrodes. In this regard, a MoS_2/DHA-PDI (dihexanoic acid-perylene-diimide) hybrid bilayer film was synthesized on FTO using spin-coating [133]. The TEM image in Fig. 7A shows the fiber-like morphology of DHA-PDI, and a flakey structure of exfoliated MoS_2. The films are optically homogeneous over a large area (Fig. 7B). Bare DHA-PDI and MoS_2 electrodes displayed low anodic photocurrent (0.25 − 0.45 mA cm^{-2}) with gradually increasing dark current towards anodic potentials in I^-/I_3^- electrolyte. Subsequently, by combining MoS_2 with DHA-PDI, higher photocurrents were achieved reaching a maximum of 2.6 mA cm^{-2}. The IPCE was also measured to investigate the light harvesting ability of electrode film (Fig. 7D). The hybrid electrode exhibited higher IPCE values than the single-component electrodes in the visible light range, and the highest efficiency of 8% was observed at 400 nm.

An SnS film was fabricated on FTO via plasma-enhanced CVD method, and it showed 100 nm thickness measured from cross-sectional field−emission scanning electron microscopy (Fig. 7E). The photovoltammogram, recorded in 0.5 M Na_2SO_4 under chopped light, suggested that SnS can show both n-type and p-type semiconductor characteristics depending on the applied potentials (Fig. 7F) [86]. Exfoliated WS_2 nanosheets were deposited on TiO_2 nanorod arrays (TiO_2 NAs), wherein TiO_2 was first deposited on FTO substrate by hydrothermal method, then exfoliated WS_2 was drop-casted on it [99]. As shown in Fig. 7G, WS_2 nanosheets are uniformly deposited on the top of TiO_2 NAs, and the TiO_2 NAs are highly ordered with the length of about 3 μm (inset of Fig. 7G). The WS_2/TiO_2 composites had a better PEC activity than the bare TiO_2 electrode towards the water oxidation reaction (Fig. 7H).

Photoelectrochemical CO_2 and N_2 reduction reaction on 2D materials

2D materials have been widely studied in PEC applications, however, only a few papers reported on the PEC CO_2 reduction reaction (CO2RR) and N_2 reduction reaction (NRR) [3, 5]. In theory, the higher CO_2 adsorption capacity, the better electron transport, and the higher density of active sites make 2D materials better suited for PEC CO2RR compared to their bulk counterparts [134]. CdSeTe nanosheets (CdSeTe NSs) were deposited on TiO_2 nanotubes by a hydrothermal method [3]. All linear sweep voltammetry (LSV) curves show a significant increase in the current

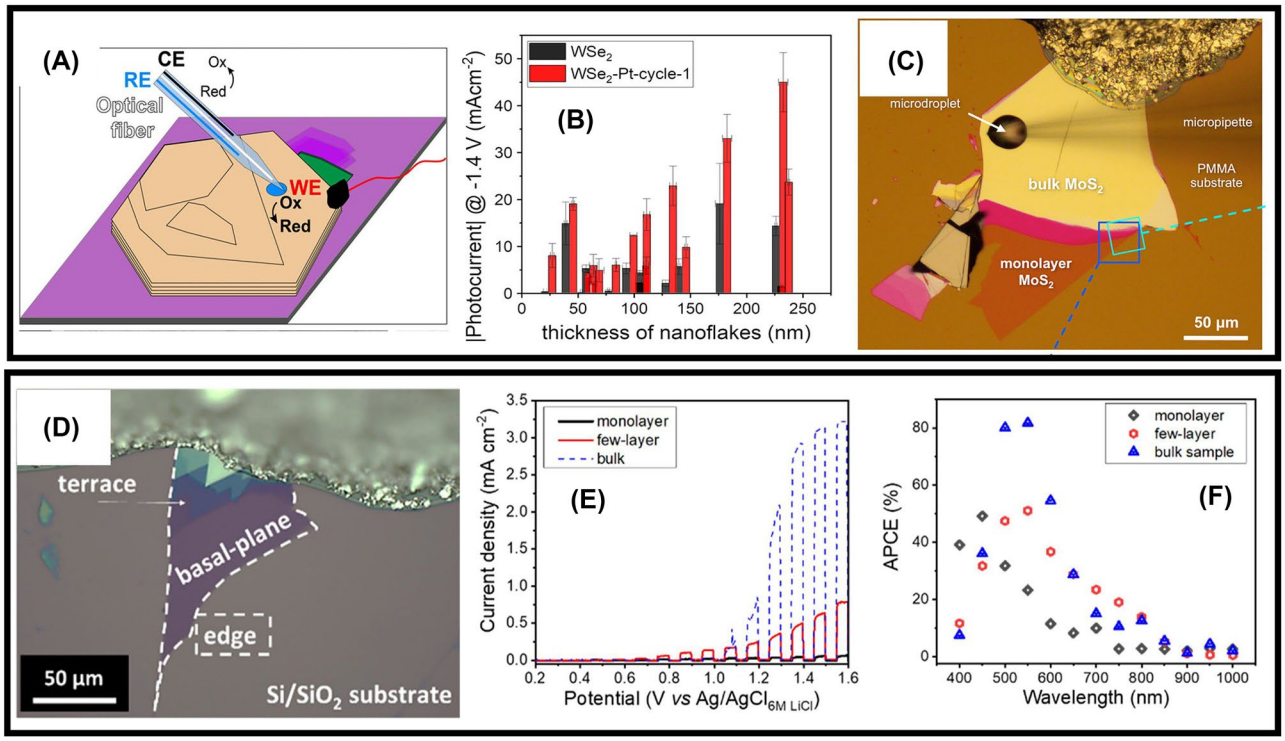

Fig. 6 **A** Scheme of a microdroplet-based PEC setup; **B** Bar chart of the photocurrent values, recorded in 1 M HCl/6 M LiCl solution for the illuminated droplets deposited on various WSe_2-Pt-cycle-1 nanoflake samples of different thickness. The irradiance was 217 mW cm^{-2}. **C** Optical micrograph of MoS_2 flake on PMMA-coated Si substrate. **D** optical micrograph of a few-layer $MoSe_2$ nanoflake, the edges are marked with white dashed lines; **E** PEC behavior of layered $MoSe_2$ specimens (basal planes), LSVs recorded for the illuminated droplets deposited on monolayer, few-layer, and bulk flakes in 6 M LiCl solution; the sweep rate was 5 mV s^{-1}; **F** absorbed photon−to−current efficiency profile, constructed using IPCE data and the estimated absorbance of the flakes. Figures adapted with permission from: **A**, **B** [131] published by John Wiley and Sons under CC BY 4.0 license; **C** [26] published by American Chemical Society under CC BY license; **D–F** [46] published by American Chemical Society under CC BY 4.0 license

density after − 0.8 V because of the competitive water reduction reaction (Fig. 8A).

After coupling the CdSeTe NSs, the current density was higher than in the case of bare TiO_2 electrode in the CO_2 saturated solution, which suggested that PEC reduction performance for CO_2 was improved upon the introduction of the CdSeTe NSs. This improvement can be credited to the flaky structure, which had an excellent electrical conductivity performance [26]. The composite showed smaller resistance (2.21 kΩ) than bare TiO_2 electrode (31.19 kΩ). The main product was methanol and its yield increased firstly and then decreased when the potential was varied from − 0.6 V to − 1.2 V, and it reached the peak at − 0.8 V. The CO2RR was dominant at potentials more positive than − 0.8 V. When the potential was more negative than − 0.8 V, the water reduction became dominant, which decreased the yield of methanol (Fig. 8B, C).

Various 2D materials were employed for PEC NRR, such as MoS_2 [2], WO_3 [6], BiOBr [4] and black phosphorus [61]. A black phosphorus electrode was fabricated by the layer−by−layer assembly of electrochemically exfoliated black phosphorus nanosheets, for PEC NRR [61]. Black phosphorus electrode exhibited better PEC performance than EC performance, and the difference was more significant at more negative potentials, as demonstrated in Fig. 8D. The optimal potential was found at − 0.4 V vs. RHE, where the highest NH_3 yield of 102.4 µg h^{-1} cm^{-2} and Faradaic efficiency of 23.3% were obtained (Fig. 8E). Long-term measurement suggested that black phosphorus electrode can give excellent stability under illumination for 12 h (Fig. 8F).

The fewer reports for 2D materials on PEC CO2RR and NRR (compared to water reduction/oxidation) could be rooted in the following reasons. 1) CO_2 and N_2 reductions are complex multi−electron processes, which are more difficult to occur than HER (only 2 electrons needed). 2) The measurement setup for PEC CO2RR and NRR requires more difficult arrangement than the other PEC applications, and the quantitative analyses of products is also rather challenging. Therefore, there is a need to further explore the applicability of 2D materials in PEC CO2RR and NRR.

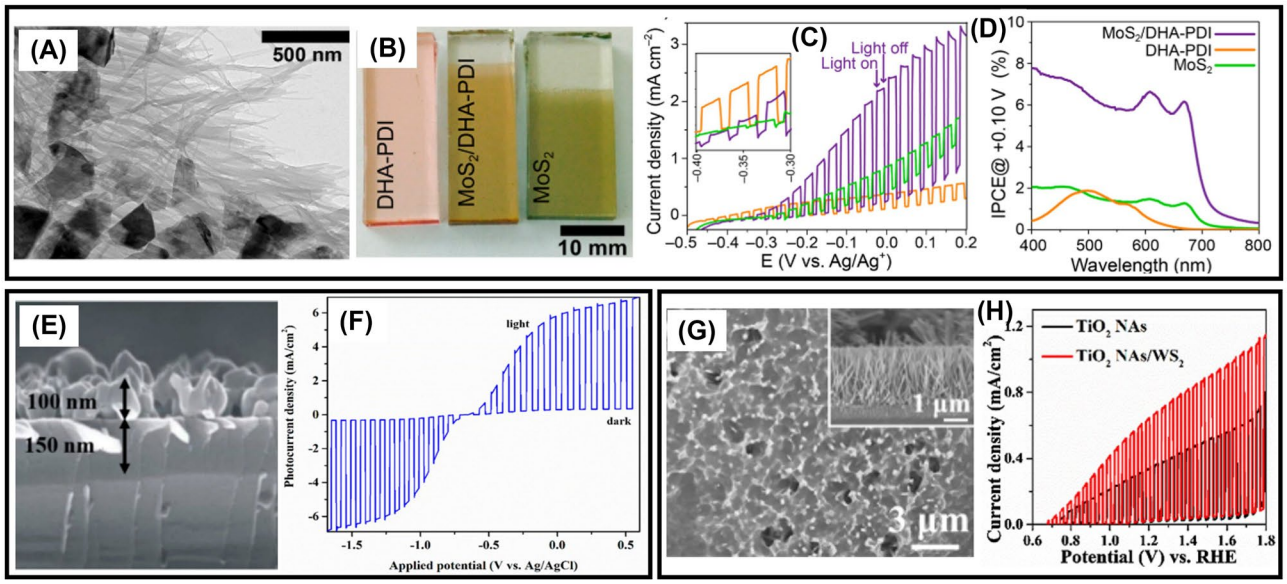

Fig. 7 **A** Morphology of MoS_2/DHA-PDI hybrid bilayer film shown by TEM; **B** photograph of the hybrid and control film deposited on FTO; **C** Current density−potential curves measured with an I^-/I_3^- redox couple under intermittent (1 Sun) illumination; **D** IPCE traces measured at + 0.1 V vs Ag/Ag^+ for solution-processed DHA-PDI, MoS_2, and MoS_2/DHA-PDI hybrid bilayer electrodes. **E** Morphology of SnS surface visualized by cross-sectional field−emission scanning electron microscopy image; **F** LSV in 0.5 M Na_2SO_4, chopped light for the SnS nanosheet photoanode at 50 mV s^{-1}. **G** SEM images of TiO_2 NAs/WS_2 composite; **H** photocurrent density under chopped AM 1.5 **G** illumination (100 mW cm^{-2}). Figures adapted with permission from: **A**–**D** [133] © 2017 American Chemical Society; **E**, **F** [86] published by MDPI under CC BY 4.0 license; **G**, **H** [99] © 2019 Elsevier

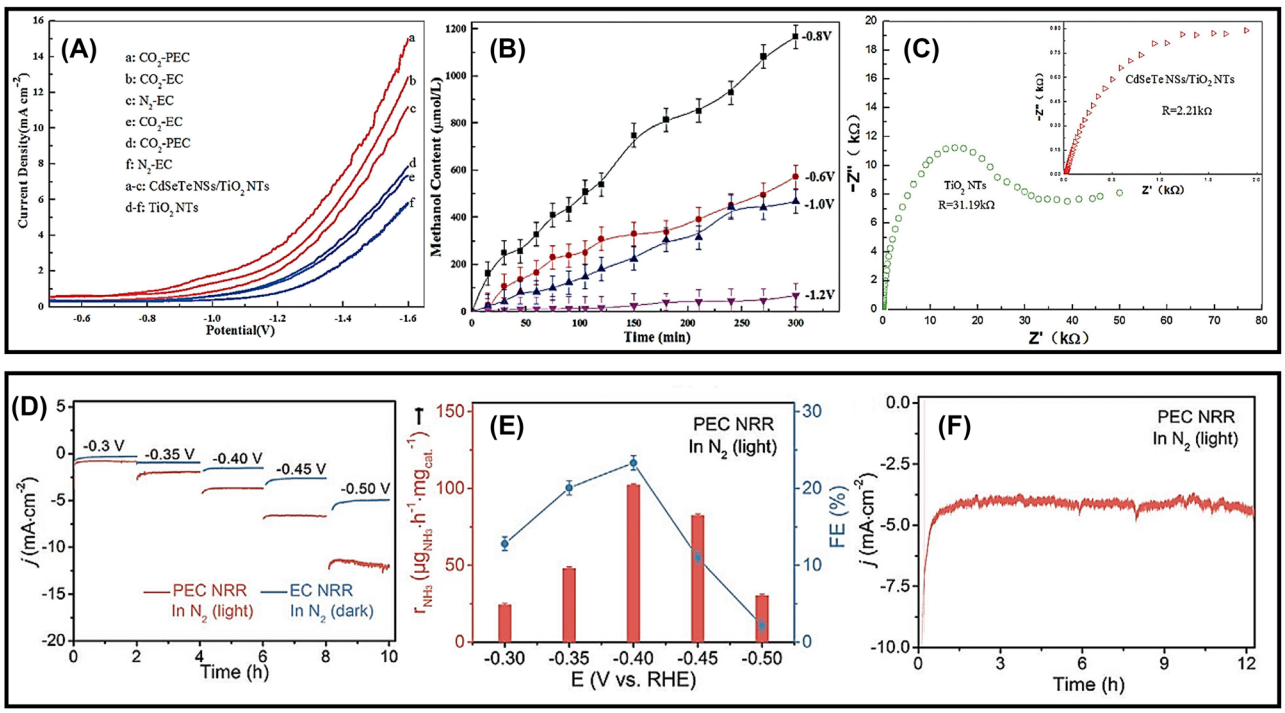

Fig. 8 **A** Current density vs. potential curves of CdSeTe NSs/TiO_2 nanotubes and TiO_2 nanotubes under 1 Sun irradiation; **B** The time-dependent curves of the methanol concentration at different potentials using CdSeTe NSs/TiO_2 nanotube photoelectrodes; **C** The electrochemical impedance spectra of TiO_2 nanotubes and CdSeTe NSs/TiO_2 nanotubes. **D** Electrochemical NRR and PEC NRR current–time curves of the black phosphorus electrode at various potentials; **E** PEC ammonia yield rates and Faradaic efficiency; **F** Current–time curve of the black phosphorus electrode recorded at − 0.4 V in a N_2 atmosphere under 1 Sun illumination. Figures adapted with permission from: **A**–**C** [3] © 2014 Royal Society of Chemistry, permission conveyed through Copyright Clearance Center, Inc; **D**–**F**) [61] © 2020 John Wiley and Sons

The passivation of defect states in 2D materials

Despite the 2D semiconductors are widely studied in PEC applications, the pristine materials generally show low PEC performance. So far, several approaches have been developed to improve PEC activity, for example the defects passivation, doping [98], loading co-catalysts [87, 88], and constructing heterojunctions [31, 54, 85]. Defects of 2D materials can act as recombination centers of charge carriers, which is detrimental to the PEC performance. Defect passivation by

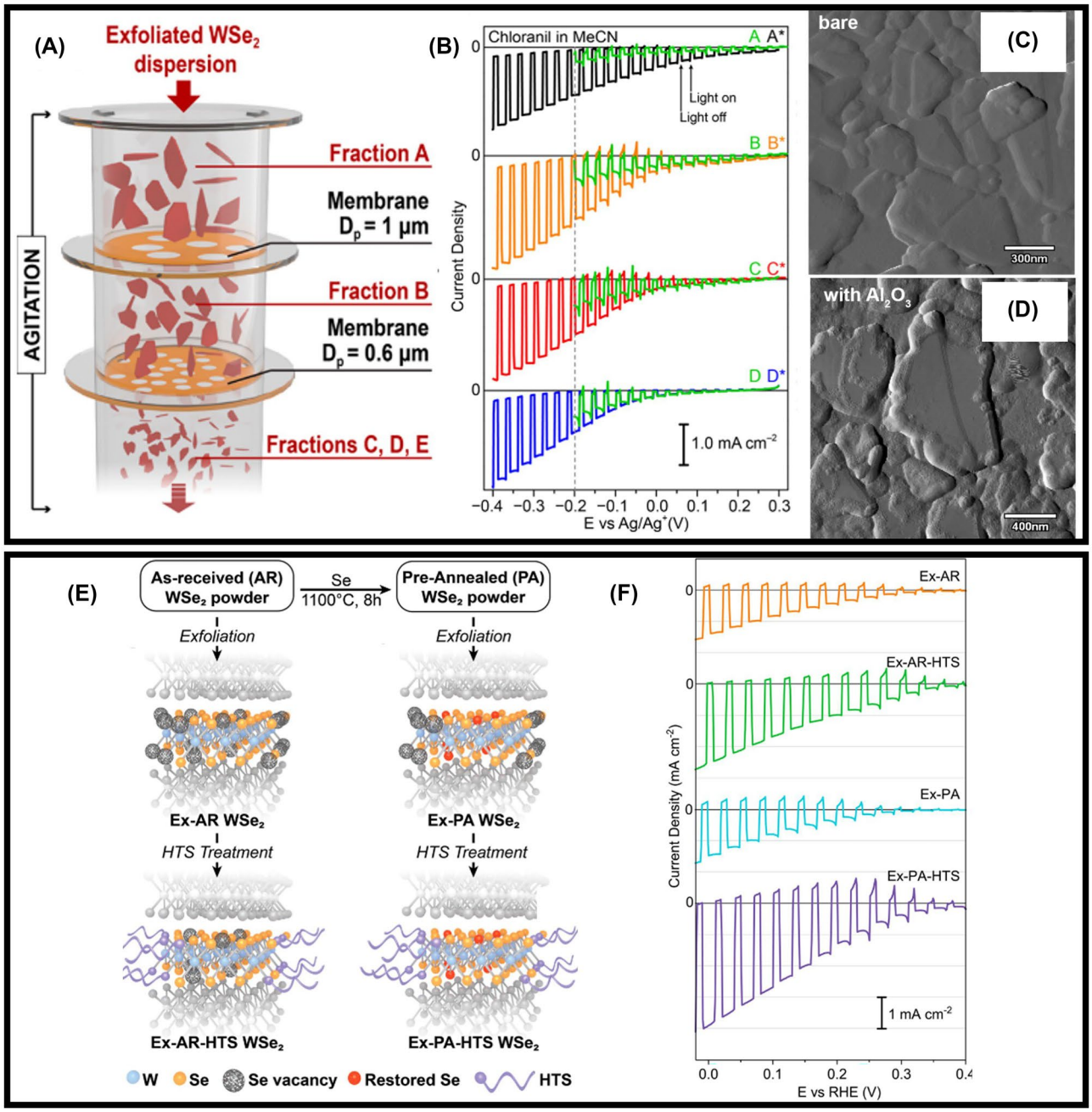

Fig. 9 **A** Schematic illustration of the multistage track-etched membrane separation column; **B** LSV curves of bare WSe_2 electrodes (electrodes **A**–**D**, green curves) and Al_2O_3-coated electrodes (Electrodes **A***–**D***, colored curves) taken at 10 mV s^{-1} under intermittent (1 Sun) illumination; Scanning probe microscope amplitude images of a WSe_2 electrode before (**C**) and after (**D**) ALD of Al_2O_3. **E** Schematic visualization of the WSe_2 flake treatments and their proposed effect on defects; **F** PEC characterizations of Pt-Cu-modified WSe_2 electrodes with preheating or post-passivation treatments or both, LSV curves scanned from positive to negative potentials (10 mV s^{-1}) under intermittent (1 Sun) illumination. Figures adapted with permission from: **A**–**D** [24] © 2017 American Chemical Society; **E**, **F** [9] © 2018 American Chemical Society

chemical methods have been explored. A flake size separation method has been employed successfully to isolate the obtained solvent-exfoliated WSe_2 flakes to 4 different fractions (fractions A−D, largest to smallest, Fig. 9A).

WSe_2 electrodes were subsequently prepared, using a modified space-confined self-assembly method [24]. They found that significant recombination happened at flake edge sites and the flake size played a critical role on the extraction of photogenerated charges. ALD-coated Al_2O_3 was used to passivate the defects of the WSe_2 flakes. After passivation, all electrodes (A*−D* in Fig. 9B) displayed significantly higher photocurrent density. The scanning probe microscopy in Fig. 9C, D suggests that the Al_2O_3 was selectively deposited on the edges of the WSe_2 flakes. The effect of intraflake and edge defects has been investigated on PEC HER performance, by applying two treatments separately: a pre-annealing before exfoliation and a post-deposition surfactant attachment, as demonstrated in Fig. 9E [9]. LSVs in Fig. 9F showed that exfoliated (Ex-AR) WSe_2 and pre-annealed (Ex-PA) WSe_2 had similar performance, which suggests that pre-exfoliation annealing alone was not effective to improve the PEC performance. After post-deposition surfactant attachment was performed, however, higher PEC performance was achieved in both cases. These results suggest that the pre-annealing treatment is indeed effective at improving the PEC performance when edge states can be passivated.

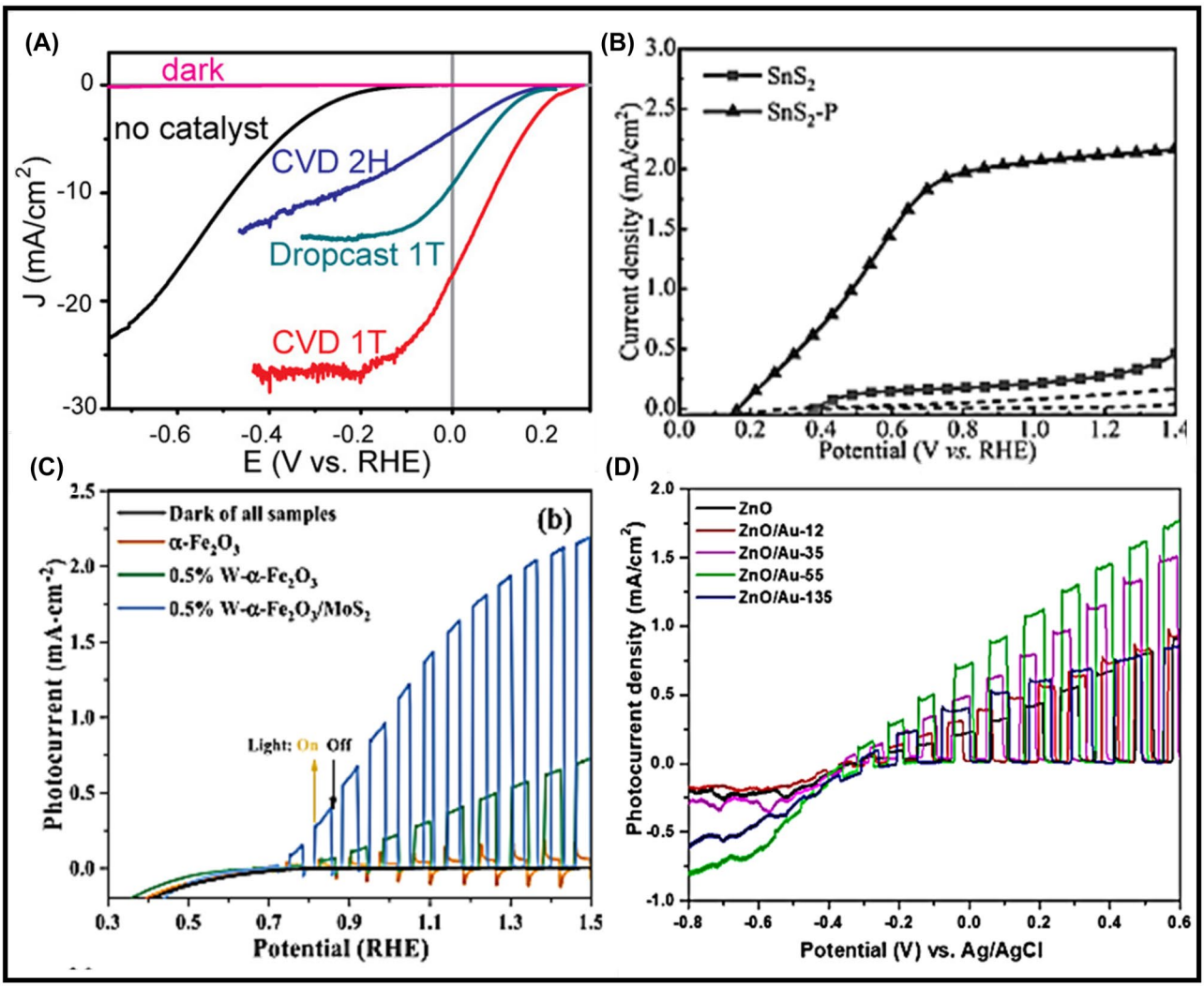

Fig. 10 **A** Current density vs. potential (vs. RHE) for CVD-grown 2H-MoS_2/Si photocathode (CVD 2H), a CVD-grown 1 T-MoS_2/Si photocathode (CVD 1 T), and a drop-casted 1 T-MoS_2/Si photocathode (dropcast 1 T) measured in 0.5 M H_2SO_4 under AM 1.5G irradiation (100 mW cm^{-2}). **B** LSV curves of SnS_2 and SnS_2-P (Ar plasma-treated sample) electrodes. **C** Chopped LSV curves for pure α-Fe_2O_3, 0.5% W:α-Fe_2O_3, and 0.5% W:α-Fe_2O_3/MoS_2 under 100 mW cm^{-2} illumination. **D** LSV curves of ZnO and ZnO/Au–n (n = 12, 35, 55, and 135 nm) under chopped 100 mW cm^{-2} illumination conditions. Figures adapted with permission from: **A** [51] © 2014 American Chemical Society; **B** [95] © 2021 American Chemical Society; **C** [98] © 2019 John Wiley and Sons; **D** [97] © 2020 American Chemical Society

Co-catalysts/heterojunctions/multilayers

The Ti- and Mo-doped WS_2 was synthesized by CVD method on FTO substrate [42]. The WS_2 electrode with Mo-doping and Ti-doping showed more than two times higher PEC performance than the electrode without doping, which is because of the metal ion doping increases the donor density in the WS_2 structure and enhances the electrical conductivity, leading to better charge transport and enhanced photocurrent density. Transition metal dichalcogenides (i.e., MoS_2, $MoSe_2$, WS_2, and WSe_2) were deposited on a pre-grown Si nanowire array as co−catalysts for HER [80]. The CVD-grown 1 T-MoS_2/Si showed a maximum of 26 mA cm^{-2} photocurrent density at − 0.4 V vs. RHE in 0.5 M H_2SO_4, and 17.6 mA cm^{-2} at 0 V vs. RHE (Fig. 10A).

The enhanced catalytic activity was attributed to the chalcogen vacancies. Hematite is one of the most promising semiconductors for PEC water oxidation reaction, however, the high charge carrier recombination rate limits its performance [111]. Therefore, MoS_2 nanosheets were synthesized by LPE method, and then drop-casted on the surface of W-doped Fe_2O_3 electrodes constructing W-doped Fe_2O_3/MoS_2 core−shell nanostructures [98]. The PEC behavior displayed in Fig. 10B indicated that the heterojunction electrode had three times higher activity than the W-doped Fe_2O_3 electrode. The improvement was ascribed to the efficient electron−hole separation due to the formed heterojunction [94, 135]. An Ar plasma-assisted strategy was used to treat SnS_2 nanosheets, which resulted in the partial reduction of Sn^{4+} to Sn^{2+}, and a SnS/SnS_2 p−n junction was formed [95]. After the Ar treatment electrode showed significantly enhanced photocurrent (Fig. 10C). Besides, the small amount of residual oxygen interacted in Ar plasma chamber with SnS/SnS_2 to form O-S bonds, which greatly reduced the overpotential of PEC water oxidation and enhance carrier transfer, boosting the PEC performance.

Decoration of semiconductor photoelectrodes with metal co-catalysts such as Pt [9, 87], Au [136, 137], and alloy [9, 81], is another viable approach to enhance PEC performance. Au nanoparticles with different sizes were dip-coated on ZnO nanosheets, and studied as photoanodes for PEC water oxidation reaction [97]. The PEC activity was dependent on the Au size (Fig. 10D). The ZnO deposited with 55 nm in diameter Au gave the highest photocurrent density, resulting from the fact that Au nanoparticles with 55 nm on ZnO increased the light absorbance of the material through the scattering effect.

Conclusions

The development of solar energy conversion devices based on 2D materials needs macroelectrodes, therefore the scale-up of electrode preparation is necessary. Unfortunately, the TMCs and other layered materials suffer from a dramatic decrease in the photocurrent, with the increase of the photoelectrode area from micrometer−scale to mm^2 or cm^2 size. In this review article, we have scrutinized different PEC processes, where 2D materials based electrodes were employed. These include both reversible model redox reactions and practically interesting processes (i.e., water splitting, CO_2, and N_2 reduction reactions). Both single crystal-based and microscopic approaches-based PEC techniques revealed the role of structural features in determining the PEC performance. In general, pure 2D semiconductors show low PEC performance, therefore different approaches have been developed to improve PEC activity (i.e., defects passivation, doping, co-catalysts, and heterojunctions). Both mono- and dichalcogenides of transition metals, and metal oxides have been studied intensively during the past decades (as discussed here), but importance of novel members of 2D family (i.e., MXenes, and double layer hydroxides) was also highlighted in this review article.

Acknowledgements The research reported in this paper is part of project no. TKP2021-NVA-19, has been implemented with the support provided by the Ministry of Innovation and Technology of Hungary from the National Research, Development and Innovation Fund, financed under the TKP2021-NVA funding scheme for financial support. This paper was also supported by the János Bolyai Research Scholarship of the Hungarian Academy of Sciences. Q.Q.B. would like to thank the Stipendium Hungaricum scholarship and the China Scholarship Council for a PhD scholarship.

Declarations

Conflict of interest The authors declare no conflict of interest. The adapted figures are used with permission of the publishers.

References

1. He J, Janáky C (2020) Recent Advances in Solar-Driven Carbon Dioxide Conversion: Expectations versus Reality. ACS Energy Lett 5:1996–2014. https://doi.org/10.1021/acsenergylett.0c00645
2. Yu MS, Jesudass SC, Surendran S et al (2022) Synergistic Interaction of MoS_2 Nanoflakes on $La_2Zr_2O_7$ Nanofibers for Improving Photoelectrochemical Nitrogen Reduction. ACS Appl Mater Interfaces 14:31889–31899. https://doi.org/10.1021/acsami.2c05653
3. Li P, Zhang J, Wang H et al (2014) The photoelectric catalytic reduction of CO_2 to methanol on CdSeTe NSs/TiO_2 NTs. Catal Sci Technol 4:1070–1077. https://doi.org/10.1039/c3cy00978e
4. Li M, Lu Q, Liu M et al (2020) Photoinduced Charge Separation via the Double-Electron Transfer Mechanism in Nitrogen Vacancies g-C_3N_5/BiOBr for the Photoelectrochemical Nitrogen Reduction. ACS Appl Mater Interfaces 12:38266–38274. https://doi.org/10.1021/acsami.0c11894
5. She H, Zhou H, Li L et al (2019) Construction of a Two-Dimensional Composite Derived from TiO_2 and SnS_2 for Enhanced Photocatalytic Reduction of CO_2 into CH_4. ACS Sustain Chem Eng 7:650–659. https://doi.org/10.1021/acssuschemeng.8b04250
6. Liu X, Shen Z, Peng X et al (2022) A photo-assisted electrochemical-based demonstrator for green ammonia synthesis. J Energy Chem 68:826–834. https://doi.org/10.1016/j.jechem.2021.12.021

7. Chhowalla M, Shin HS, Eda G et al (2013) The chemistry of two-dimensional layered transition metal dichalcogenide nanosheets. Nat Chem 5:263–275. https://doi.org/10.1038/nchem.1589
8. Manzeli S, Ovchinnikov D, Pasquier D et al (2017) 2D transition metal dichalcogenides. Nat Rev Mater 2:17033. https://doi.org/10.1038/natrevmats.2017.33
9. Yu X, Guijarro N, Johnson M, Sivula K (2018) Defect Mitigation of Solution-Processed 2D WSe_2 Nanoflakes for Solar-to-Hydrogen Conversion. Nano Lett 18:215–222. https://doi.org/10.1021/acs.nanolett.7b03948
10. Yang W, Park J, Kwon HC et al (2020) Solar water splitting exceeding 10% efficiency: Via low-cost Sb_2Se_3 photocathodes coupled with semitransparent perovskite photovoltaics. Energy Environ Sci 13:4362–4370. https://doi.org/10.1039/d0ee02959a
11. Asadi M, Kumar B, Behranginia A et al (2014) Robust carbon dioxide reduction on molybdenum disulphide edges. Nat Commun 5:4470. https://doi.org/10.1038/ncomms5470
12. Patel AB, Machhi HK, Chauhan P et al (2019) Electrophoretically Deposited $MoSe_2$/WSe_2 Heterojunction from Ultrasonically Exfoliated Nanocrystals for Enhanced Electrochemical Photoresponse. ACS Appl Mater Interfaces 11:4093–4102. https://doi.org/10.1021/acsami.8b18177
13. Vanka S, Wang Y, Ghamari P et al (2018) A High Efficiency Si Photoanode Protected by Few-Layer $MoSe_2$. Sol RRL 2:1–6. https://doi.org/10.1002/solr.201800113
14. Yang W, Zhang X, Tilley SD (2021) Emerging Binary Chalcogenide Light Absorbers: Material Specific Promises and Challenges. Chem Mater 33:3467–3489. https://doi.org/10.1021/acs.chemmater.1c00741
15. Kautek W, Gobrecht J, Gerischer H (1980) Applicability of Semiconducting Layered Materials for Electrochemical Solar Energy Conversion. Berichte der Bunsengesellschaft/Physical Chem Chem Phys 84:1034–1040. https://doi.org/10.1002/bbpc.19800841021
16. Lewerenz HJ, Heller A, DiSalvo FJ (1980) Relationship between surface morphology and solar conversion efficiency of tungsten diselenide photoanodes. J Am Chem Soc 102:1877–1880. https://doi.org/10.1021/ja00526a019
17. Fan FRF, White HS, Wheeler BL, Bard AJ (1980) Semiconductor Electrodes. 31. Photoelectrochemistry and Photovoltaic Systems with n- and p-Type WSe_2 in Aqueous Solution. J Am Chem Soc 102:5142–5148. https://doi.org/10.1021/ja00536a002
18. Kautek W, Gerischer H (1982) Anisotropic photocorrosion of n-type MoS_2 $MoSe_2$, and WSe_2 single crystal surfaces: the role of cleavage steps, line and screw dislocations. Surf Sci 119:46–60. https://doi.org/10.1016/0039-6028(82)90186-8
19. Abruna HD, Bard AJ (1982) Semiconductor Electrodes. 44. Photoelectrochemistry at Polycrystalline p-Type WSe_2 Films. J Electrochem Soc 129:673–675. https://doi.org/10.1149/1.2123949
20. Novoselov KS, Geim AK, Morozov SV et al (2004) Electric field in atomically thin carbon films. Science 306(80-):666–669. https://doi.org/10.1126/science.1102896
21. Novoselov KS, Fal'ko VI, Colombo L et al (2012) A roadmap for graphene. Nature 490:192–200. https://doi.org/10.1038/nature11458
22. Mokaya R (2000) Ion Exchange | Novel Layered Materials: Non-Phosphates. In: Encyclopedia of Separation Science. pp 1610–1617
23. Peng B, Ang PK, Loh KP (2015) Two-dimensional dichalcogenides for light-harvesting applications. Nano Today 10:128–137. https://doi.org/10.1016/j.nantod.2015.01.007
24. Yu X, Sivula K (2017) Photogenerated Charge Harvesting and Recombination in Photocathodes of Solvent-Exfoliated WSe_2. Chem Mater 29:6863–6875. https://doi.org/10.1021/acs.chemmater.7b02018
25. Velický M, Toth PS (2017) From two-dimensional materials to their heterostructures: An electrochemist's perspective. Appl Mater Today 8. https://doi.org/10.1016/j.apmt.2017.05.003
26. Velický M, Bissett MA, Woods CR et al (2016) Photoelectrochemistry of Pristine Mono- and Few-Layer MoS_2. Nano Lett 16:2023–2032. https://doi.org/10.1021/acs.nanolett.5b05317
27. Anasori B, Lukatskaya MR, Gogotsi Y (2017) 2D metal carbides and nitrides (MXenes) for energy storage. Nat Rev Mater 2:16098. https://doi.org/10.1038/natrevmats.2016.98
28. Naguib M, Kurtoglu M, Presser V et al (2011) Two-Dimensional Nanocrystals Produced by Exfoliation of Ti_3AlC_2. Adv Mater 23:4248–4253. https://doi.org/10.1002/adma.201102306
29. Zuo Y, Liu Y, Li J et al (2019) Solution-Processed Ultrathin SnS_2-Pt Nanoplates for Photoelectrochemical Water Oxidation. ACS Appl Mater Interfaces 11:6918–6926. https://doi.org/10.1021/acsami.8b17622
30. Taniguchi T, Nurdiwijayanto L, Ma R, Sasaki T (2022) Chemically exfoliated inorganic nanosheets for nanoelectronics. Appl Phys Rev 9:021313. https://doi.org/10.1063/5.0083109
31. Kaur N, Ghosh A, Ahmad M et al (2022) Increased visible light absorption and charge separation in 2D–3D In_2S_3-ZnO heterojunctions for enhanced photoelectrochemical water splitting. J Alloys Compd 903:164007. https://doi.org/10.1016/j.jallcom.2022.164007
32. Mahala C, Sharma MD, Basu M (2019) ZnO@CdS heterostructures: An efficient photoanode for photoelectrochemical water splitting. New J Chem 43:7001–7010. https://doi.org/10.1039/c9nj01373c
33. Frindt RF, Yoffe AD, Bowden FP (1963) Physical properties of layer structures : optical properties and photoconductivity of thin crystals of molybdenum disulphide. Proc R Soc London Ser A Math Phys Sci 273:69–83. https://doi.org/10.1098/rspa.1963.0075
34. Yun WS, Han SW, Hong SC et al (2012) Thickness and strain effects on electronic structures of transition metal dichalcogenides: 2H-MX_2 semiconductors (M = Mo, W; X = S, Se, Te). Phys Rev B - Condens Matter Mater Phys 85:33305. https://doi.org/10.1103/PhysRevB.85.033305
35. Ye Y, Xian Y, Cai J et al (2019) Linear and Nonlinear Optical Properties of Few-Layer Exfoliated SnSe Nanosheets. Adv Opt Mater 7:1800579. https://doi.org/10.1002/adom.201800579
36. Kim D, Park K, Shojaei F et al (2019) Thickness-dependent bandgap and electrical properties of GeP nanosheets. J Mater Chem A 7:16526–16532. https://doi.org/10.1039/c9ta04470a
37. Ye W, He C, Asim Mushtaq M et al (2022) High Performance Cobalt-Vanadium Layered Double Hydroxide Nanosheets for Photoelectrochemical Reduction of Nitrogen. Eur J Inorg Chem. https://doi.org/10.1002/ejic.202200325
38. Hernandez Y, Nicolosi V, Lotya M et al (2008) High-yield production of graphene by liquid-phase exfoliation of graphite. Nat Nanotechnol 3:563–568. https://doi.org/10.1038/nnano.2008.215
39. Cai Y, Zhang G, Zhang Y-W (2014) Layer-dependent Band Alignment and Work Function of Few-Layer Phosphorene. Sci Rep 4:6677. https://doi.org/10.1038/srep06677
40. Bonaccorso F, Lombardo A, Hasan T et al (2012) Production and processing of graphene and 2d crystals. Mater Today 15:564–589. https://doi.org/10.1016/S1369-7021(13)70014-2
41. Ramanathan S, Gopinath SCB, Arshad MKM et al (2020) Nanoparticle synthetic methods: Strength and limitations. INC
42. Ahmadi A, Zargar Shoushtari M (2019) Enhancing the photoelectrochemical water splitting performance of WS_2 nanosheets by doping titanium and molybdenum via a low temperature CVD method. J Electroanal Chem 849:113361. https://doi.org/10.1016/j.jelechem.2019.113361
43. Sherrell PC, Palczynski P, Sokolikova MS et al (2019) Large-Area CVD MoS_2/WS_2 Heterojunctions as a Photoelectrocatalyst for Salt-Water Oxidation. ACS Appl Energy Mater 2:5877–5882. https://doi.org/10.1021/acsaem.9b01008

44. Wang J, Su J, Guo L (2016) Controlled Aqueous Growth of Hematite Nanoplate Arrays Directly on Transparent Conductive Substrates and Their Photoelectrochemical Properties. Chem An Asian J 11:2328–2334. https://doi.org/10.1002/asia.201600888
45. Bonaccorso F, Bartolotta A, Coleman JN, Backes C (2016) 2D-Crystal-Based Functional Inks. Adv Mater 28:6136–6166. https://doi.org/10.1002/adma.201506410
46. Tóth PS, Szabó G, Janáky C (2021) Structural Features Dictate the Photoelectrochemical Activities of Two-Dimensional $MoSe_2$ and WSe_2 Nanostructures. J Phys Chem C 125:7701–7710. https://doi.org/10.1021/acs.jpcc.1c01265
47. Kwon KC, Choi S, Hong K et al (2016) Wafer-scale transferable molybdenum disulfide thin-film catalysts for photoelectrochemical hydrogen production. Energy Environ Sci 9:2240–2248. https://doi.org/10.1039/C6EE00144K
48. Nicolosi V, Chhowalla M, Kanatzidis MG et al (2013) Liquid exfoliation of layered materials. Science (80-) 340:72–75. https://doi.org/10.1126/science.1226419
49. Bellani S, Bartolotta A, Agresti A et al (2021) Solution-processed two-dimensional materials for next-generation photovoltaics. Chem Soc Rev 50:11870–11965. https://doi.org/10.1039/d1cs00106j
50. Gómez H, Maldonado A, Asomoza R et al (1997) Characterization of indium-doped zinc oxide films deposited by pyrolytic spray with different indium compounds as dopants. Thin Solid Films 293:117–123. https://doi.org/10.1016/S0040-6090(96)09001-3
51. Ding Q, Meng F, English CR et al (2014) Efficient photoelectrochemical hydrogen generation using heterostructures of Si and chemically exfoliated metallic MoS_2. J Am Chem Soc 136:8504–8507. https://doi.org/10.1021/ja5025673
52. Trung TN, Seo DB, Quang ND et al (2018) Enhanced photoelectrochemical activity in the heterostructure of vertically aligned few-layer MoS_2 flakes on ZnO. Electrochim Acta 260:150–156. https://doi.org/10.1016/j.electacta.2017.11.089
53. Hussain S, Hussain S, Waleed A et al (2017) Spray Pyrolysis Deposition of $ZnFe_2O_4/Fe_2O_3$ Composite Thin Films on Hierarchical 3-D Nanospikes for Efficient Photoelectrochemical Oxidation of Water. J Phys Chem C 121:18360–18368. https://doi.org/10.1021/acs.jpcc.7b05266
54. Zhang F, Chen Y, Zhou W et al (2019) Hierarchical $SnS_2/CuInS_2$ Nanosheet Heterostructure Films Decorated with C60 for Remarkable Photoelectrochemical Water Splitting. ACS Appl Mater Interfaces 11:9093–9101. https://doi.org/10.1021/acsami.8b21222
55. Sopha H, Tesfaye AT, Zazpe R et al (2019) ALD growth of MoS_2 nanosheets on TiO_2 nanotube supports. FlatChem 17:100130. https://doi.org/10.1016/j.flatc.2019.100130
56. Martella C, Melloni P, Cinquanta E et al (2016) Engineering the Growth of MoS_2 via Atomic Layer Deposition of Molybdenum Oxide Film Precursor. Adv Electron Mater 2:1600330. https://doi.org/10.1002/aelm.201600330
57. Hussain SA, Dey B, Bhattacharjee D, Mehta N (2018) Unique supramolecular assembly through Langmuir – Blodgett (LB) technique. Heliyon 4:e01038. https://doi.org/10.1016/j.heliyon.2018.e01038
58. Oliveira ON, Caseli L, Ariga K (2022) The Past and the Future of Langmuir and Langmuir-Blodgett Films. Chem Rev 122:6459–6513. https://doi.org/10.1021/acs.chemrev.1c00754
59. Cunningham G, Khan U, Backes C et al (2013) Photoconductivity of solution-processed MoS_2 films. J Mater Chem C 1:6899–6904. https://doi.org/10.1039/C3TC31402B
60. Lee H, Yang W, Tan J et al (2020) High-Performance Phase-Pure SnS Photocathodes for Photoelectrochemical Water Splitting Obtained via Molecular Ink-Derived Seed-Assisted Growth of Nanoplates. ACS Appl Mater Interfaces 12:15155–15166. https://doi.org/10.1021/acsami.9b23045
61. Liu D, Wang J, Bian S et al (2020) Photoelectrochemical Synthesis of Ammonia with Black Phosphorus. Adv Funct Mater 30. https://doi.org/10.1002/adfm.202002731
62. Moreira J, Vale AC, Alves NM (2021) Spin-coated freestanding films for biomedical applications. J Mater Chem B 9:3778–3799. https://doi.org/10.1039/d1tb00233c
63. David S, Mahadik MA, An GW et al (2018) Effect of directional light dependence on enhanced photoelectrochemical performance of $ZnIn_2S_4/TiO_2$ binary heterostructure photoelectrodes. Electrochim Acta 276:223–232. https://doi.org/10.1016/j.electacta.2018.04.110
64. Kim DH, Park JC, Park J et al (2021) Wafer-Scale Growth of a MoS_2 Monolayer via One Cycle of Atomic Layer Deposition: An Adsorbate Control Method. Chem Mater 33:4099–4105. https://doi.org/10.1021/acs.chemmater.1c00729
65. Bianca G, Zappia MI, Bellani S et al (2020) Liquid-phase exfoliated gese nanoflakes for photoelectrochemical- type photodetectors and photoelectrochemical water splitting. ACS Appl Mater Interfaces 12:48598–48613. https://doi.org/10.1021/acsami.0c14201
66. Carey T, Jones C, Le Moal F et al (2018) Spray-Coating Thin Films on Three-Dimensional Surfaces for a Semitransparent Capacitive-Touch Device. ACS Appl Mater Interfaces 10:19948–19956. https://doi.org/10.1021/acsami.8b02784
67. Wong M, Ishige R, White KL et al (2014) Large-scale self-assembled zirconium phosphate smectic layers via a simple spray-coating process. Nat Commun 5:1–12. https://doi.org/10.1038/ncomms4589
68. Habibi M, Ahmadian-Yazdi M-R, Eslamian M (2017) Optimization of spray coating for the fabrication of sequentially deposited planar perovskite solar cells. J Photonics Energy 7:022003. https://doi.org/10.1117/1.jpe.7.022003
69. Lv X, Yu L, Li F et al (2021) Penta-MS_2 (M = Mn, Ni, Cu/Ag and Zn/Cd) monolayers with negative Poisson's ratios and tunable bandgaps as water-splitting photocatalysts. J Mater Chem A 9:6993–7004. https://doi.org/10.1039/d1ta00019e
70. Torrisi SB, Singh AK, Montoya JH et al (2020) Two-dimensional forms of robust CO_2 reduction photocatalysts. npj 2D Mater Appl 4:24. https://doi.org/10.1038/s41699-020-0154-y
71. Fujishima A, Honda K (1972) Electrochemical photolysis of water at a semiconductor electrode. Nature 238:37–38. https://doi.org/10.1038/238037a0
72. Li D, Shi J, Li C (2018) Transition-Metal-Based Electrocatalysts as Cocatalysts for Photoelectrochemical Water Splitting: A Mini Review. Small 14:1–22. https://doi.org/10.1002/smll.201704179
73. Hisatomi T, Kubota J, Domen K (2014) Recent advances in semiconductors for photocatalytic and photoelectrochemical water splitting. Chem Soc Rev 43:7520–7535. https://doi.org/10.1039/c3cs60378d
74. Yang H, Nan C, Gao N et al (2022) Three-phase interface of SnO_2 nanoparticles loaded on hydrophobic MoS_2 enhance photoelectrochemical N_2 reduction. Electrochim Acta 430:141086. https://doi.org/10.1016/j.electacta.2022.141086
75. Yu Y, Huang S-Y, Li Y et al (2014) Layer-Dependent Electrocatalysis of MoS_2 for Hydrogen Evolution. Nano Lett 14:553–558. https://doi.org/10.1021/nl403620g
76. Giri B, Masroor M, Yan T et al (2019) Balancing Light Absorption and Charge Transport in Vertical SnS_2 Nanoflake Photoanodes with Stepped Layers and Large Intrinsic Mobility. Adv Energy Mater 9. https://doi.org/10.1002/aenm.201901236
77. Zhao H, Zhang H, Liu G et al (2019) Ultra-small colloidal heavy-metal-free nanoplatelets for efficient hydrogen generation. Appl Catal B Environ 250:234–241. https://doi.org/10.1016/j.apcatb.2019.03.028

78. Yang W, Park J, Kwon HC et al (2020) Solar water splitting exceeding 10% efficiency: Via low-cost Sb_2Se_3photocathodes coupled with semitransparent perovskite photovoltaics. Energy Environ Sci 13:4362–4370. https://doi.org/10.1039/d0ee02959a
79. Park J, Yang W, Tan J et al (2020) Hierarchal Nanorod-Derived Bilayer Strategy to Enhance the Photocurrent Density of Sb_2Se_3 Photocathodes for Photoelectrochemical Water Splitting. ACS Energy Lett 5:136–145. https://doi.org/10.1021/acsenergylett.9b02486
80. Kwak IH, Kwon IS, Lee JH et al (2021) Chalcogen-vacancy group VI transition metal dichalcogenide nanosheets for electrochemical and photoelectrochemical hydrogen evolution. J Mater Chem C 9:101–109. https://doi.org/10.1039/d0tc04715e
81. McKone JR, Pieterick AP, Gray HB, Lewis NS (2013) Hydrogen Evolution from Pt/Ru-Coated p-Type WSe_2 Photocathodes. J Am Chem Soc 135:223–231. https://doi.org/10.1021/ja308581g
82. Roy K, Maitra S, Ghosh D et al (2022) 2D-Heterostructure assisted activation of MoS_2 basal plane for enhanced photoelectrochemical hydrogen evolution reaction. Chem Eng J 435:134963. https://doi.org/10.1016/j.cej.2022.134963
83. Hu D, Xiang J, Zhou Q et al (2018) One-step chemical vapor deposition of MoS_2 nanosheets on SiNWs as photocathodes for efficient and stable solar-driven hydrogen production. Nanoscale 10:3518–3525. https://doi.org/10.1039/c7nr09235k
84. Seo S, Kim S, Choi H et al (2019) Direct In Situ Growth of Centimeter-Scale Multi-Heterojunction $MoS_2/WS_2/WSe_2$ Thin-Film Catalyst for Photo-Electrochemical Hydrogen Evolution. Adv Sci 6. https://doi.org/10.1002/advs.201900301
85. Xu X, Liu Y, Zhu Y et al (2017) Fabrication of a $Cu_2O/g\text{-}C_3N_4/WS_2$ Triple-Layer Photocathode for Photoelectrochemical Hydrogen Evolution. ChemElectroChem 4:1498–1502. https://doi.org/10.1002/celc.201700014
86. Huang X, Woo H, Lee D et al (2021) High-efficiency photon-capturing capability of two-dimensional sns nanosheets for photoelectrochemical cells. Catalysts 11:1–9. https://doi.org/10.3390/catal11020236
87. Ma Z, Konze P, Küpers M et al (2020) Elucidation of the Active Sites for Monodisperse FePt and Pt Nanocrystal Catalysts for p-WSe_2 Photocathodes. J Phys Chem C 124:11877–11885. https://doi.org/10.1021/acs.jpcc.0c01288
88. Monny SA, Zhang L, Wang Z et al (2020) Fabricating highly efficient heterostructured $CuBi_2O_4$ photocathodes for unbiased water splitting. J Mater Chem A 8:2498–2504. https://doi.org/10.1039/c9ta10975g
89. Xu XY, Dong XF, Bao ZJ et al (2017) Three electron channels toward two types of active sites in MoS_2@Pt nanosheets for hydrogen evolution. J Mater Chem A 5:22654–22661. https://doi.org/10.1039/c7ta07241d
90. Yu X, Prévot MS, Guijarro N, Sivula K (2015) Self-assembled 2D WSe_2 thin films for photoelectrochemical hydrogen production. Nat Commun 6. https://doi.org/10.1038/ncomms8596
91. Chaudhary P, Ingole PP (2020) In-Situ solid-state synthesis of 2D/2D interface between Ni/NiO hexagonal nanosheets supported on g-C_3N_4 for enhanced photo-electrochemical water splitting. Int J Hydrogen Energy 45:16060–16070. https://doi.org/10.1016/j.ijhydene.2020.04.011
92. Tayebi M, Masoumi Z, Kolaei M et al (2022) Highly efficient and stable WO_3/MoS_2-MoO_x photoanode for photoelectrochemical hydrogen production; a collaborative approach of facet engineering and P-N junction. Chem Eng J 446:136830. https://doi.org/10.1016/j.cej.2022.136830
93. Li H, Yang C, Wang X et al (2020) Mixed 3D/2D dimensional TiO_2 nanoflowers/$MoSe_2$ nanosheets for enhanced photoelectrochemical hydrogen generation. J Am Ceram Soc 103:1187–1196. https://doi.org/10.1111/jace.16807
94. Ghasemi F, Hassanpour Amiri M (2021) Facile in situ fabrication of rGO/MoS_2 heterostructure decorated with gold nanoparticles with enhanced photoelectrochemical performance. Appl Surf Sci 570:151228. https://doi.org/10.1016/j.apsusc.2021.151228
95. Meng L, Zhou X, Wang S et al (2019) A Plasma-Triggered O−S Bond and P−N Junction Near the Surface of a SnS_2 Nanosheet Array to Enable Efficient Solar Water Oxidation. Angew Chemie Int Ed 58:16668–16675. https://doi.org/10.1002/anie.201910510
96. Karmakar K, Maity D, Pal D et al (2020) Photo-Induced Exciton Dynamics and Broadband Light Harvesting in ZnO Nanorod-Templated Multilayered Two-Dimensional MoS_2/MoO_3 Photoanodes for Solar Fuel Generation. ACS Appl Nano Mater 3:1223–1231. https://doi.org/10.1021/acsanm.9b01972
97. Mahala C, Sharma MD, Basu M (2020) Near-Field and Far-Field Plasmonic Effects of Gold Nanoparticles Decorated on ZnO Nanosheets for Enhanced Solar Water Splitting. ACS Appl Nano Mater 3:1153–1165. https://doi.org/10.1021/acsanm.9b01678
98. Masoumi Z, Tayebi M, Kolaei M et al (2021) Simultaneous Enhancement of Charge Separation and Hole Transportation in a W:α-Fe_2O_3/MoS_2 Photoanode: A Collaborative Approach of MoS_2 as a Heterojunction and W as a Metal Dopant. ACS Appl Mater Interfaces 13:39215–39229. https://doi.org/10.1021/acsami.1c08139
99. Pi Y, Liu B, Li Z et al (2019) TiO_2 nanorod arrays decorated with exfoliated WS_2 nanosheets for enhanced photoelectrochemical water oxidation. J Colloid Interface Sci 545:282–288. https://doi.org/10.1016/j.jcis.2019.03.041
100. Mahala C, Sharma MD, Basu M (2020) ZnO Nanosheets Decorated with Graphite-Like Carbon Nitride Quantum Dots as Photoanodes in Photoelectrochemical Water Splitting. ACS Appl Nano Mater 3:1999–2007. https://doi.org/10.1021/acsanm.0c00081
101. Masoumi Z, Tayebi M, Kolaei M, Lee BK (2022) Unified surface modification by double heterojunction of MoS_2 nanosheets and $BiVO_4$ nanoparticles to enhance the photoelectrochemical water splitting of hematite photoanode. J Alloys Compd 890:161802. https://doi.org/10.1016/j.jallcom.2021.161802
102. Masoumi Z, Tayebi M, Lee BK (2021) Ultrasonication-assisted liquid-phase exfoliation enhances photoelectrochemical performance in α-Fe_2O_3/MoS_2 photoanode. Ultrason Sonochem 72:105403. https://doi.org/10.1016/j.ultsonch.2020.105403
103. Pulipaka S, Koushik AKS, Boni N et al (2019) Tin disulfide based ternary composites for visible light driven photoelectrochemical water splitting. Int J Hydrogen Energy 44:11584–11592. https://doi.org/10.1016/j.ijhydene.2019.03.135
104. Zhang S, Liu Y, Feng M et al (2021) Leaf-like MXene nanosheets intercalated TiO_2 nanorod array photoelectrode with enhanced photoelectrochemical performance. J Power Sources 484:229236. https://doi.org/10.1016/j.jpowsour.2020.229236
105. Yin H, Wang Y, Ma L et al (2022) Effect of surface-deposited $Ti_3C_2T_x$ MXene on the photoelectrochemical water-oxidation performance of iron-doped titania nanorod array. Chem Eng J 431:134124. https://doi.org/10.1016/j.cej.2021.134124
106. Zhong C, Shang Z, Zhao C et al (2022) Co-Catalyst $Ti_3C_2T_x$ MXene-Modified ZnO Nanorods Photoanode for Enhanced Photoelectrochemical Water Splitting. Top Catal. https://doi.org/10.1007/s11244-022-01619-0
107. Seo DB, Dongquoc V, Jayarathna RA et al (2022) Rational heterojunction design of 1D WO_3 nanorods decorated with vertical 2D MoS_2 nanosheets for enhanced photoelectrochemical performance. J Alloys Compd 911:165090. https://doi.org/10.1016/j.jallcom.2022.165090
108. Li L, Shi H, Yu H et al (2021) Ultrathin $MoSe_2$ nanosheet anchored CdS-ZnO functional paper chip as a highly efficient tandem Z-scheme heterojunction photoanode for scalable photoelectrochemical water

splitting. Appl Catal B Environ 292:120184. https://doi.org/10.1016/j.apcatb.2021.120184
109. Suryawanshi MP, Ghorpade UV, Shin SW et al (2018) Facile, Room Temperature, Electroless Deposited (Fe_{1-x}, M_nx)OOH Nanosheets as Advanced Catalysts: The Role of Mn Incorporation. Small 14:1–8. https://doi.org/10.1002/smll.201801226
110. Kong Z, Zhang J, Wang H et al (2020) Constructing 1D/2D heterojunction photocatalyst from $FeSe_2$ nanorods and $MoSe_2$ nanoplates with high photocatalytic and photoelectrochemical performance. Int J Energy Res 44:1205–1217. https://doi.org/10.1002/er.5014
111. Ratnayake SP, Ren J, Murdoch BJ et al (2022) Nanostructured Electrodes Based on Two-Dimensional SnO_2 for Photoelectrochemical Water Splitting. ACS Appl Energy Mater 5:10359–10365. https://doi.org/10.1021/acsaem.2c01087
112. Zhang D, Yang S, Fang X et al (2022) In situ localization of $BiVO_4$ onto two-dimensional MXene promoting photoelectrochemical nitrogen reduction to ammonia. Chinese Chem Lett 33:4669–4674. https://doi.org/10.1016/j.cclet.2022.02.001
113. Bai Y, Bai H, Qu K et al (2019) In-situ approach to fabricate BiOI photocathode with oxygen vacancies: Understanding the N_2 reduced behavior in photoelectrochemical system. Chem Eng J 362:349–356. https://doi.org/10.1016/j.cej.2019.01.051
114. Ye W, Arif M, Fang X et al (2019) Efficient Photoelectrochemical Route for the Ambient Reduction of N_2 to NH_3 Based on Nanojunctions Assembled from MoS_2 Nanosheets and TiO_2. ACS Appl Mater Interfaces 11:28809–28817. https://doi.org/10.1021/acsami.9b06596
115. Chen Z, Forman AJ, Jaramillo TF (2013) Bridging the gap between bulk and nanostructured photoelectrodes: The impact of surface states on the electrocatalytic and photoelectrochemical properties of MoS_2. J Phys Chem C 117:9713–9722. https://doi.org/10.1021/jp311375k
116. Brownson DAC, Munro LJ, Kampouris DK, Banks CE (2011) Electrochemistry of graphene: not such a beneficial electrode material? RSC Adv 1:978–988. https://doi.org/10.1039/C1RA00393C
117. Velický M, Bradley DF, Cooper AJ et al (2014) Electron transfer kinetics on mono- and multilayer graphene. ACS Nano 8:10089–10100. https://doi.org/10.1021/nn504298r
118. Todt MA, Isenberg AE, Nanayakkara SU et al (2018) Single-Nanoflake Photo-Electrochemistry Reveals Champion and Spectator Flakes in Exfoliated $MoSe_2$ Films. J Phys Chem C 122:6539–6545. https://doi.org/10.1021/acs.jpcc.7b12715
119. Lewerenz HJ, Gerischer H, Lübke M (1984) Photoelectrochemistry of WSe_2 Electrodes: Comparison of Stepped and Smooth Surfaces. J Electrochem Soc 131:100–104. https://doi.org/10.1149/1.2115467
120. Velazquez JM, John J, Esposito DV et al (2016) A scanning probe investigation of the role of surface motifs in the behavior of p-WSe_2 photocathodes. Energy Environ Sci 9:164–175. https://doi.org/10.1039/C5EE02530C
121. Velický M, Bissett MA, Toth PS et al (2015) Electron transfer kinetics on natural crystals of MoS_2 and graphite. Phys Chem Chem Phys 17:17844–17853. https://doi.org/10.1039/c5cp02490k
122. Toth PS, Velický M, Bissett MA et al (2016) Asymmetric MoS_2/Graphene/Metal Sandwiches: Preparation, Characterization, and Application. Adv Mater 28:8256–8264. https://doi.org/10.1002/adma.201600484
123. Toth PS, Valota AT, Velický M et al (2014) Electrochemistry in a drop: A study of the electrochemical behaviour of mechanically exfoliated graphene on photoresist coated silicon substrate. Chem Sci 5:582–589. https://doi.org/10.1039/c3sc52026a
124. Eisenberg D (2015) Imaging the Anisotropic Reactivity of a Tungsten Diselenide Photocathode. ChemElectroChem 2:1259–1263. https://doi.org/10.1002/celc.201500103
125. Hill JW, Hill CM (2019) Directly Mapping Photoelectrochemical Behavior within Individual Transition Metal Dichalcogenide Nanosheets. Nano Lett 19:5710–5716. https://doi.org/10.1021/acs.nanolett.9b02336
126. Bentley CL, Kang M, Maddar FM et al (2017) Electrochemical maps and movies of the hydrogen evolution reaction on natural crystals of molybdenite (MoS_2): basal vs. edge plane activity. Chem Sci 8:6583–6593. https://doi.org/10.1039/C7SC02545A
127. Tao B, Unwin PR, Bentley CL (2020) Nanoscale Variations in the Electrocatalytic Activity of Layered Transition-Metal Dichalcogenides. J Phys Chem C 124:789–798. https://doi.org/10.1021/acs.jpcc.9b10279
128. Edwards MA, Bertoncello P, Unwin PR (2009) Slow Diffusion Reveals the Intrinsic Electrochemical Activity of Basal Plane Highly Oriented Pyrolytic Graphite Electrodes. J Phys Chem C 113:9218–9223. https://doi.org/10.1021/jp8092918
129. Zhou W, Zou X, Najmaei S et al (2013) Intrinsic Structural Defects in Monolayer Molybdenum Disulfide. Nano Lett 13:2615–2622. https://doi.org/10.1021/nl4007479
130. Jaramillo TF, Jørgensen KP, Bonde J et al (2007) Identification of Active Edge Sites for Electrochemical H_2 Evolution from MoS_2 Nanocatalysts. Science (80-) 317:100–102. https://doi.org/10.1126/science.1141483
131. Tóth PS, Szabó G, Bencsik G et al (2022) Peeling off the surface: Pt-decoration of WSe_2 nanoflakes results in exceptional photoelectrochemical HER activity. SusMat 2:749–760. https://doi.org/10.1002/sus2.86
132. Bozheyev F, Harbauer K, Ellmer K (2017) Highly (001)-textured p-type WSe_2 Thin Films as Efficient Large-Area Photocathodes for Solar Hydrogen Evolution. Sci Rep 7:16003. https://doi.org/10.1038/s41598-017-16283-8
133. Yu X, Rahmanudin A, Jeanbourquin XA et al (2017) Hybrid heterojunctions of solution-processed semiconducting 2D transition metal dichalcogenides. ACS Energy Lett 2:524–531. https://doi.org/10.1021/acsenergylett.6b00707
134. Bi W, Wu C, Xie Y (2018) Atomically Thin Two-Dimensional Solids: An Emerging Platform for CO_2 Electroreduction. ACS Energy Lett 3:624–633. https://doi.org/10.1021/acsenergylett.7b01343
135. Hassan MA, Kim MW, Johar MA et al (2019) Transferred monolayer MoS_2 onto GaN for heterostructure photoanode: Toward stable and efficient photoelectrochemical water splitting. Sci Rep 9. https://doi.org/10.1038/s41598-019-56807-y
136. Yin Z, Chen B, Bosman M et al (2014) Au nanoparticle-modified MoS_2 nanosheet-based photoelectrochemical cells for water splitting. Small 10:3537–3543. https://doi.org/10.1002/smll.201400124
137. Ali A, Mangrio FA, Chen X et al (2019) Ultrathin MoS_2 nanosheets for high-performance photoelectrochemical applications: Via plasmonic coupling with Au nanocrystals. Nanoscale 11:7813–7824. https://doi.org/10.1039/c8nr10320h